NURETH14-xxx

VALIDATION OF POST-DRYOUT PHENOMENA FOR THE SPACE CODE

K. D. Kim, S. K. Moon, B. J. Kim and S. W. Lee
Korea Atomic Energy Research Institute
1045 Daedeokdaero, Yuseong-gu, Daejeon, Korea

Abstract

SPACE code which is based on a multi-dimensional two-fluid, three-field model is under development for the licensing calculation of pressurized water reactors. Unlike other major best-estimate nuclear reactor system analysis codes that have been developed based on a two-fluid six equation model, the field equations of SPACE code incorporates a dispersed liquid field in addition to vapor and continuous liquid fields. This model features a set of nine equations of mass, energy and momentum conservation. A dispersed liquid field is expected to be important in annular-mist and post-dryout conditions since a dispersed liquid field behaves differently with a continuous liquid field. This is the major reason to incorporate a dispersed liquid field as an additional liquid field. As a part of the validation effort of SPACE code, FLECHT-SEASET reflood problems have been assessed and are presented in this paper.

Introduction

The Ministry of Commerce and Industry and Energy (MOCIE) has launched a nuclear reactor thermal hydraulic system analysis code development program for licensing calculations of pressurized water reactors. SPACE (Safety and Performance Analysis Code) code is under development based on a multi-dimensional two-fluid, three-field model. A separate set of mass, energy and momentum equations are solved for each field (gas, continuous liquid, and dispersed droplet), with closure relations to account for mass, energy and momentum transfer between fields [1].

An accurate prediction of a post-dryout condition is important since this condition occurs during blowdown, refill and reflood phases of a loss of coolant accident (LOCA). The current generation thermal-hydraulic codes for LOCA analysis use a 2-fluid, 2-field equation model that includes a gas field and liquid field. These codes are not able to capture the dispersed droplet behaviour which has different characteristics from continuous liquid field. The dispersed droplet in annular-mist and post-dryout conditions has a large interface area and different velocities compared to a continuous liquid field.

A CHF(Critical Heat Flux) prediction based on a look-up table has become common in many best-estimate codes. SPACE code also uses an AECL (Atomic Energy of Canada Limited) CHF look-up table for CHF prediction [2]. In addition, SPACE adopts the AECL look-up table for the prediction of film boiling heat transfer. Transition boiling heat transfer coefficient is determined based on an interpolation between CHF and film boiling heat transfer rate at the minimum film boiling temperature. The minimum film boiling temperature calculated by the Carbajo model [3] is used as a boundary between transition and film boiling heat transfer regimes.

This paper shows the post-dryout wall-to-fluid heat transfer model, droplet entrainment/ deposition model, and interface drag model, along with preliminary assessment results of SPACE code.

1. Physical closure relations

1.1 Wall-to-fluid heat transfer

During a LOCA, the wall-to-fluid heat transfer rate in post-CHF regions is very important to predict a peak cladding temperature and quenching time. Due to its accuracy and extensibility, the latest AECL look-up table (LUT) is selected for SPACE code. A CHF temperature is used to define the boundary between nucleate boiling and transition boiling regions. The CHF temperature is calculated iteratively by using the nucleate boiling model:

$$T_{CHF} = T_{sat} + q''_{CHF} / h_{NB}(T_{CHF}) .$$

Some post-CHF heat transfer models in the SPACE code were taken from COBRA/TRAC [4].

Transition boiling is an unstable heat transfer region that has both nucleate boiling and film boiling characteristics. SPACE code for a transition boiling heat flux uses an interpolation scheme between the CHF and minimum film boiling point heat flux based on wetted-wall fraction such as

$$q''_{TB} = \max(0.2, 1-\alpha_g) \cdot \delta \cdot q''_{CHF} + q''_{FB}$$

where $\delta = \left(\dfrac{T_w - T_{\min}}{T_{CHF} - T_{\min}} \right)^2$.

Also, minimum film boiling temperature, which is a boundary between transition boiling and film boiling, is calculated by the Carbajo model.

The film boiling heat transfer mechanisms are composed of conduction across the vapour film to continuous liquid, convection to vapor, and radiation into all three fields. A film boiling look-up table [5] is used to obtain an overall film boiling heat flux. To partition the total heat flux into three fields, the heat flux to each field is calculated by the appropriate correlations. The heat flux to a vapour phase by convection is estimated by a Dittus-Boelter correlation and the conduction heat flux to a continuous liquid by a Bromley correlation [6]. Heat transfer due to droplet striking the wall is calculated using the modified Forslund-Rohsenow correlation [7]. Three radiation heat fluxes are obtained by the radiation model of Sun et al. [8]. Total heat flux obtained by a look-up table is partitioned proportional to the calculated heat flux to each phase by correlations. During a reflood condition, the pool boiling CHF by Zuber correlation weighed with a liquid fraction and ratio of wall temperature to saturated temperature is added to a continuous liquid heat flux.

1.2 Droplet entrainment during reflood

Droplet entrainment for a bottom quench front point is estimated by a model used in COBRA/TRAC. This model postulates that droplets are formed by bubbles breaking in the liquid pool. The entrainment rate is given by

$$S_E = \left(\frac{\alpha_g v_g}{v_{crit}} \right)^2 \dot{m}_g - (\text{droplet inlet flow rate}) ,$$

where $\dot{m}_g$ is the vertical vapour mass flow rate and v_{crit} is the critical vapour velocity to lift a droplet with radius defined by the Weber number against gravity. The critical vapour velocity is given by

$$v_{crit} = \left(\frac{4\,We_d}{3\,C_D}\right)^{1/4} \left(\frac{\sigma\, g(\rho_l - \rho_g)}{\rho_g^2}\right)^{1/4} .$$

A Weber number and drag coefficient of 2.7 and 0.45, respectively, are used as COBRA/TRAC.

1.3 Interfacial drag model

Interfacial drags exist at the interfaces between the gas and droplets, and between the gas and continuous liquid. In SPACE code, drag-coefficient models are used to calculate the droplet-gas interfacial drag and the continuous liquid-gas interfacial drag for vertical annular flow, whereas the drift-flux model is preferred for vertical bubbly/slug flow. In a bundle region, a modified version of the Bestion model proposed by Analytis [9] is used for low pressure, pre-dryout conditions.

$$V_{gj} = 0.124\sqrt{\frac{g(\rho_l - \rho_g)D_h}{\rho_g}}$$

Coddington & Macian [10] reported that the Bestion model [11] predicted the experimental data reasonably well over a wide range of void fractions when the distribution parameter was set to unity. SPACE code incorporates their findings. The drag coefficient for an inverted annular flow is assumed to be a constant of 0.01 as in COBRA/TRAC. The drag coefficient accounting for the effects of multiple ligaments given by Clift et al. [12] and Richardson & Zaki [13] is used in an inverted slug region. For dispersed liquid-gas interfacial drag, the Ishii & Chawla [14] correlation is used.

2. Code validation against FLECHT-SEASET Experiments

2.1 Description of FLECHT-SEASET experiment facility

To assess the post-CHF model and reflood model, the FLECHT-SEASET tests [15] were chosen because the tesst were performed using a real size fuel bundle similar to a typical Westinghouse 17X17 fuel bundle. The test section of the FLECHT-SEASET test facility consisted of 161 heater rods and 16 thimble rods with a square lattice array in a 0.194 m diameter cylindrical housing as shown in Fig. 1. The bundle also comprised 4 instrumented thimbles, and 8 solid triangular fillers except rods. The length of the active heater rods was 3.66 m long. Along the axial direction of the rod bundle, 8 spacer grids were installed. A Kanthal heater coil imbedded in boron nitride was used to heat the rods, which had stainless steel cladding. The outside diameter and wall thickness of the heater rod were 9.5 mm and 0.64 mm, respectively. The rod-to-rod pitch was 12.6 mm, and each rod had a cosine axial power profile.

2.2 SPACE Modelling

Figure 2 shows a nodalization scheme for a FLECHT-SEASET assessment. Only the heated section is modelled by a pipe component 115 with 20 equal length axial nodes. Other parts of the test facility were modelled as boundary conditions. The pipe outlet is modelled as a pressure boundary of TFBC (Temporal face boundary condition) 110 to control the system pressure, and the inlet is modelled as a flow boundary of TFBC 120 to adjust the reflood injection rate. The spacer grids were modelled by specifying a form loss coefficient of 1.2 at the location of the real bottom elevations of the spacer grids.

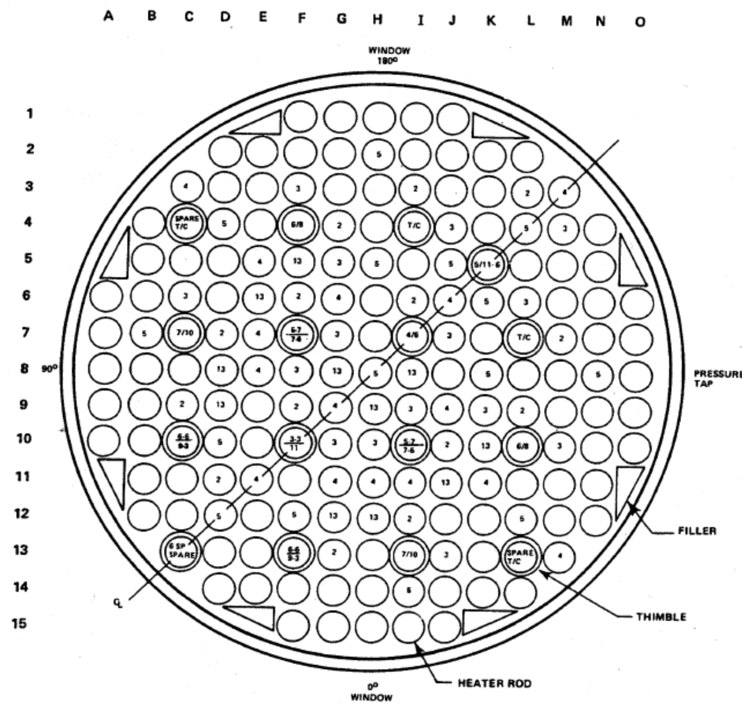

Figure 1. Cross section of FLECHT-SEASET test facility

Five heat structures were used to model the active heater rods, unheated rods, filler rods, thimbles, and housing wall. The active and unheated heater rods are modelled with 7 radial nodes: 1 node for boron nitride inside Kanthal heater coil, 1 for Kanthal heater coil, 2 for boron nitride outside heater coil, and 3 for stainless steel cladding. The power source was modelled with a general table. The heat transfer enhancement due to spacer grids was ignored for simplicity.

Initially, the test section was filled with superheated steam. At time 0 s, reflood water is injected from the bottom of the test section, TFBC 120. It is known that an axial heat conduction of the heat structure can be significant near the quench front location due to large wall temperature difference. However, the effect of axial heat conduction is less than 5% of the radial heat conduction according to our parametric study. One-dimensional heat conduction for the radial direction only was considered for this simulation.

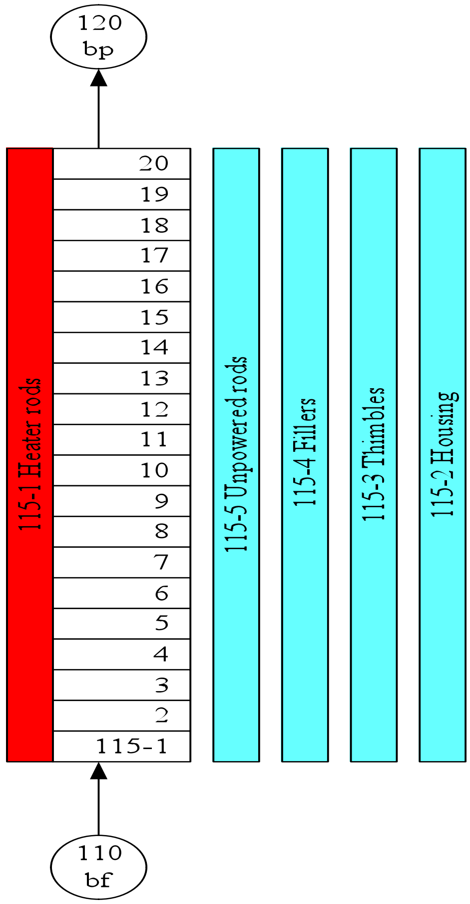

Figure 2. SPACE modelling for FLECHT-SEASET experiment

2.3 Assessment results

Among the tests performed at the FLECHT-SEASET test facility, two data sets were selected to evaluate the post-dry out heat transfer calculation capability of SPACE code. Their test conditions are presented in Table 1. Runs 31504, 31302 and 31701 were selected as these tests represent reflood tests with low, medium and high force flooding rates. These tests had the same initial rod power and same initial wall temperature distribution.

The assessments were initiated at the time of the initial cold water injection into the test section. To evaluate the predictive capability of the code, the SPACE calculation result was compared with measurement data and the calculation results of RELAP5/MOD3.3 for both runs.

Table 1. The selected FLECHT-SEASET tests for SPACE assessment

Test conditions	31504	31302	31701
Flooding rate (cm/s)	2.40	7.65	15.50
Upper plenum pressure (MPa)	0.28	0.28	0.28
Reflood water temperature (°C)	51	52	53
Inlet subcooling (°C)	79	78	77
Initial rod peak power (kW/m)	2.3	2.3	2.3

Figure 3 shows the predicted integrated water injection and discharge flows of the test section. The total integrated water discharge flow agrees well with the measured flow for run 31504. The integrated droplet flow shown with the red line with the triangle is smaller than expected. This might be affected by the droplet entrainment/deposition models. Figures 4 though 8 compare the predicted wall temperatures by SPACE with the experimental data and RELAP5 calculations for various elevations. SPACE predicts reasonably the wall temperature behaviour and quenching times. Both SPACE and RELAP5 calculations shows earlier quenching than the experiment as the elevation increases. Figures 9 and 10 compare the predicted vapour temperatures by SPACE with the experimental data and RELAP5/MOD3.3 calculations for two different elevations. For both SPACE and RELAP5 calculations, the predicted vapour temperatures were predicted to be lower than the measurement.

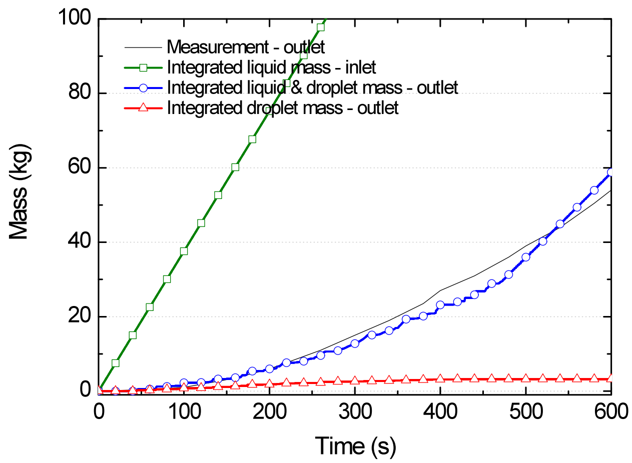

Figure 3. Integrated water discharge flow

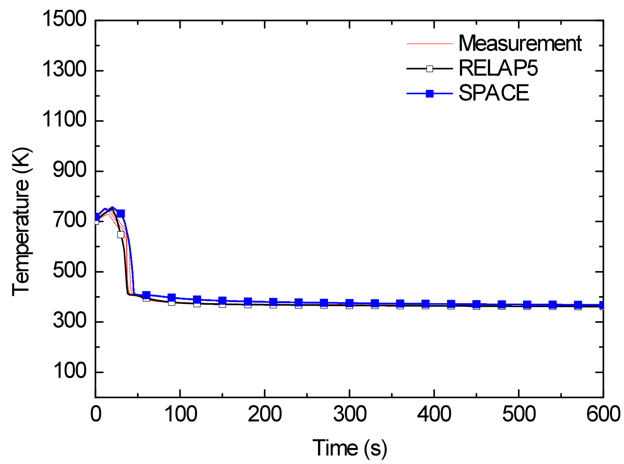

Figure 4. Clad temperature at 2 ft

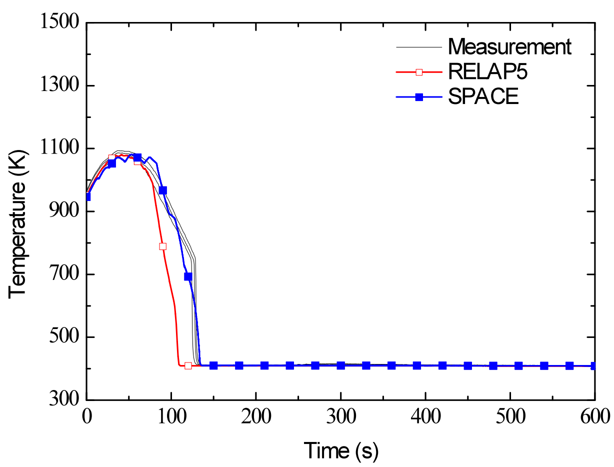

Figure 5. Clad temperature at 4 ft

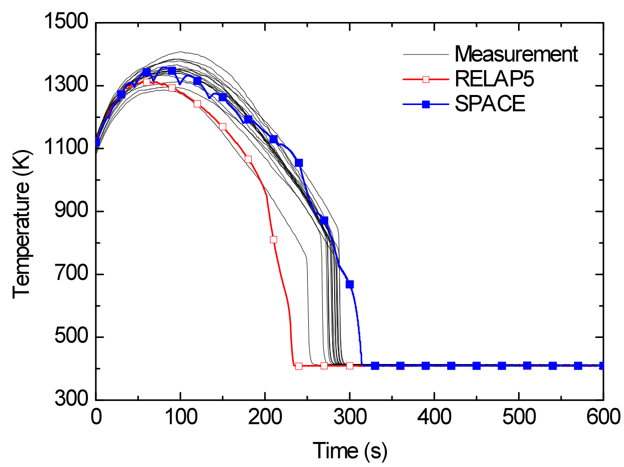

Figure 6. Clad temperature at 6 ft

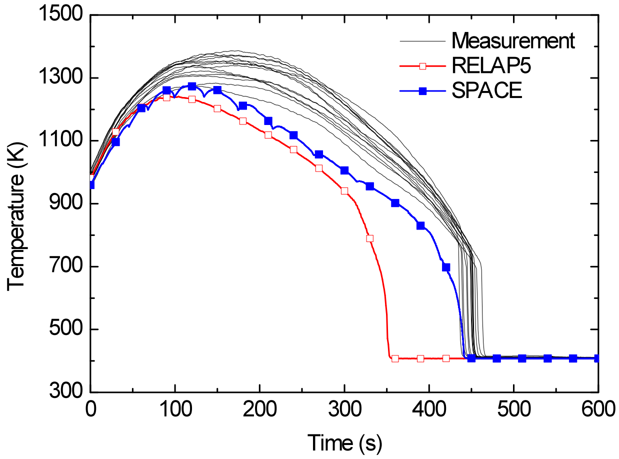

Figure 7. Clad temperature at 8 ft

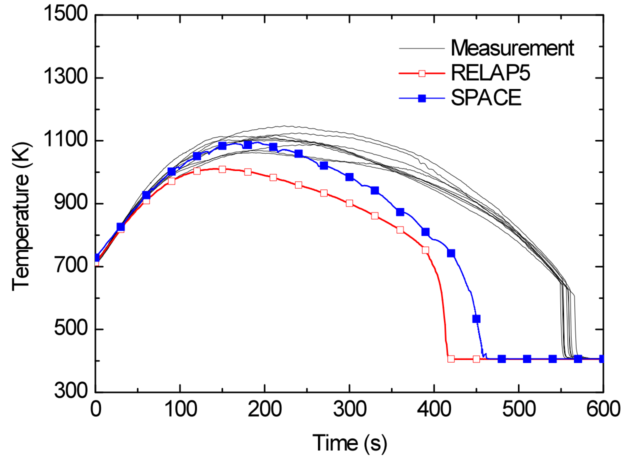

Figure 8. Clad temperature at 10 ft

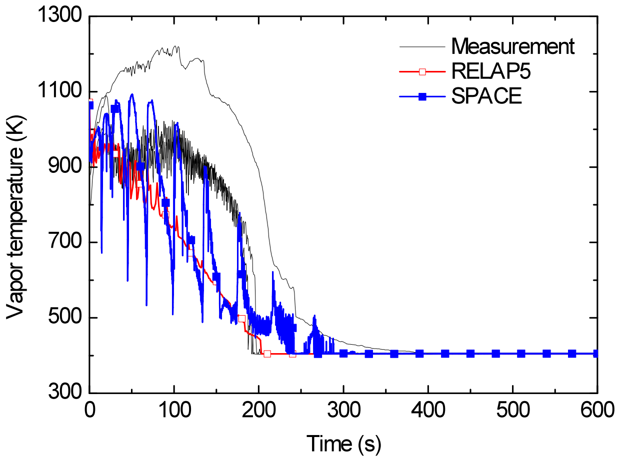

Figure 9. Vapour temperature at 6 ft

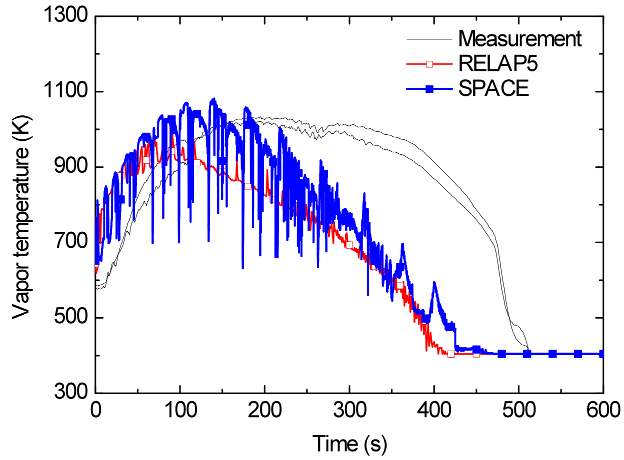

Figure 10. Vapour temperature at 10 ft

Figures 11 though 15 compare the predicted wall temperatures with the experimental data and RELAP5 calculations for various elevations for run 31302. For the case of medium flooding velocity, run 31302, SPACE predicts well the wall temperature behaviour and quenching times except at high elevation. Figure 16 shows a comparison of the calculated carryout liquid mass with the measured data. The calculated carryout liquid mass is larger than the measured data. The same behaviour is examined in a high flooding case of run 31701 as shown in Fig. 22. This is mainly due to the poor prediction of the interface frictional force. Although the modified Bestion model predicts interface frictional force very well for a low flow condition, it may over-predict the interface frictional force for a high flow condition.

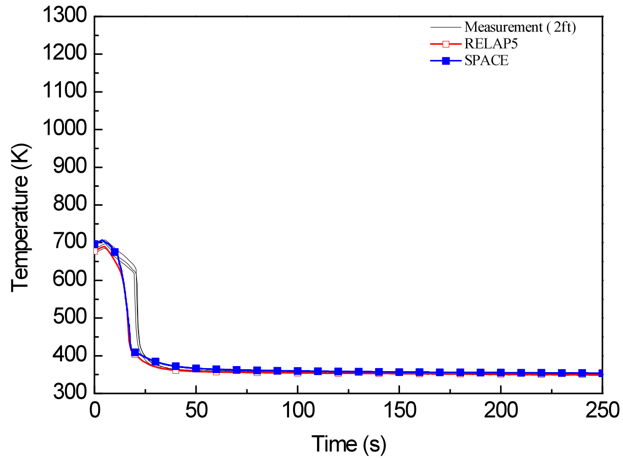

Figure 11. Clad temperature at 2 ft

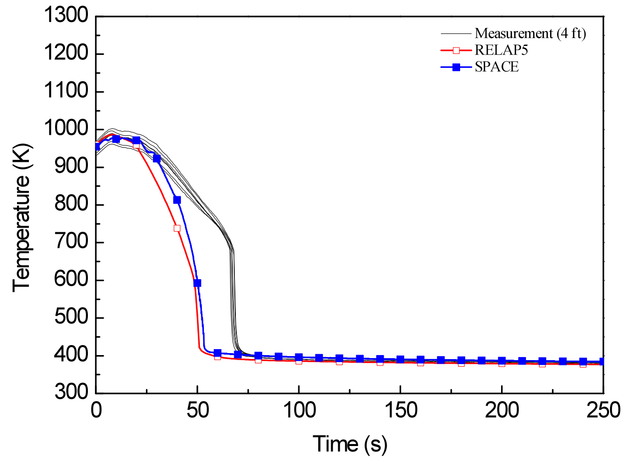

Figure 12. Clad temperature at 4 ft

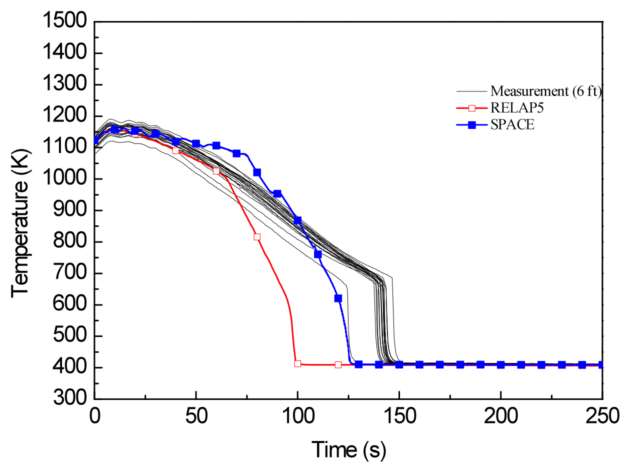

Figure 13. Clad temperature at 6 ft

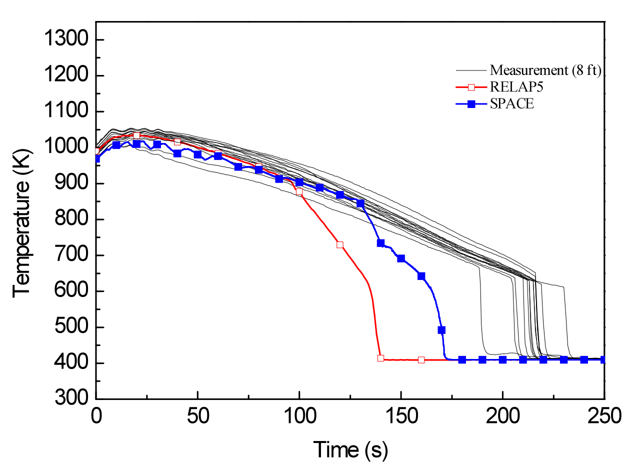

Figure 14. Clad temperature at 8 ft

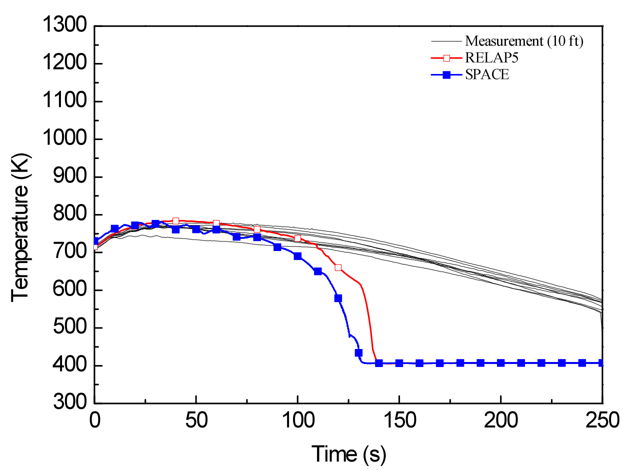

Figure 15. Clad temperature at 10 ft

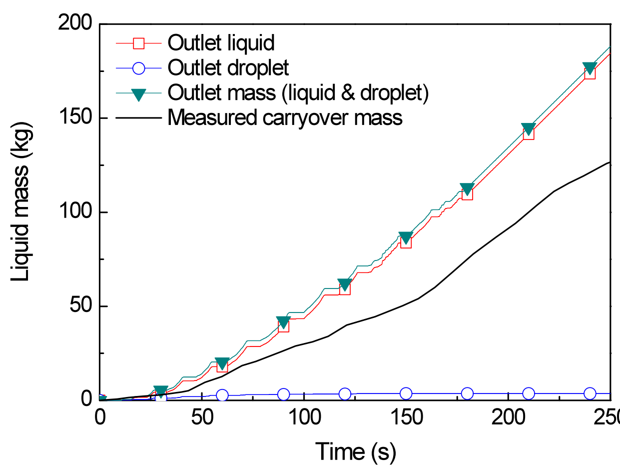

Figure 16. Carryout liquid mass

Figures 17 though 21 compare the predicted wall temperatures with the experimental data and RELAP5 calculations for various elevations for run 31701. For a case of high flooding velocity, run 31701, SPACE predicts well the wall temperature behaviour and quenching times. The calculated quenching time at high elevation occurs earlier than experiment data as mentioned before.

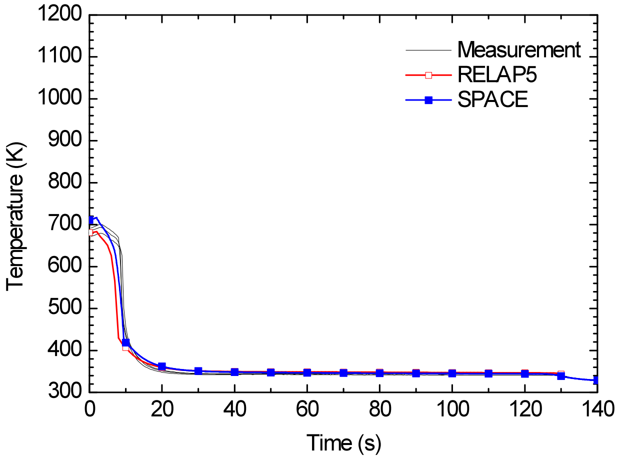

Figure 17. Clad temperature at 2 ft

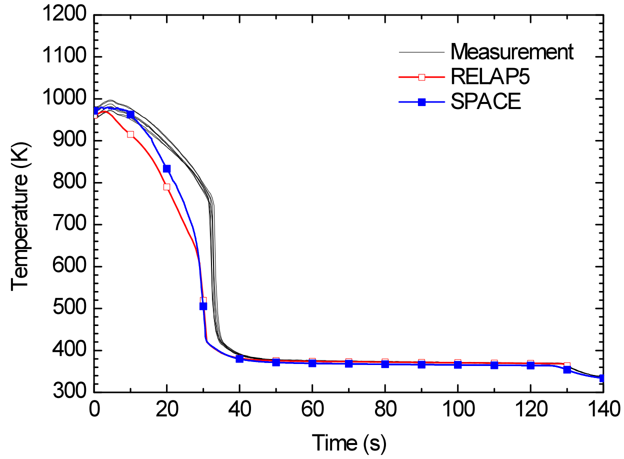

Figure 18. Clad temperature at 4 ft

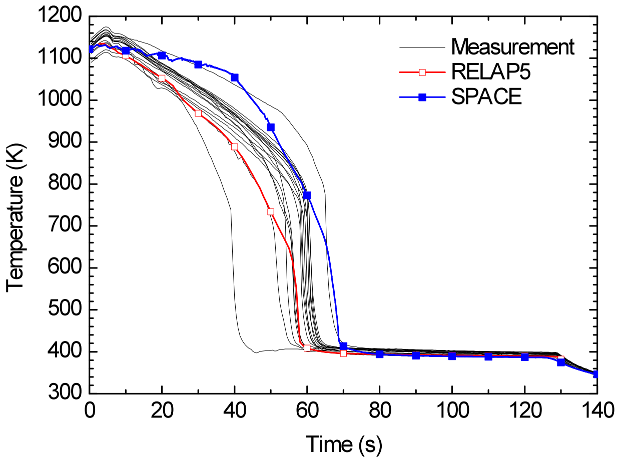

Figure 19. Clad temperature at 6 ft

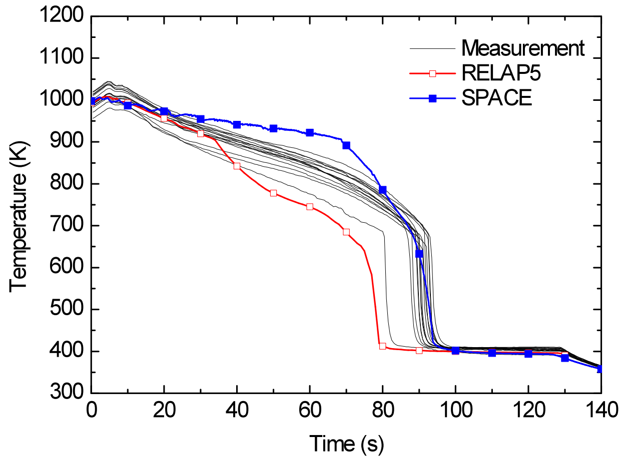

Figure 20. Clad temperature at 8 ft

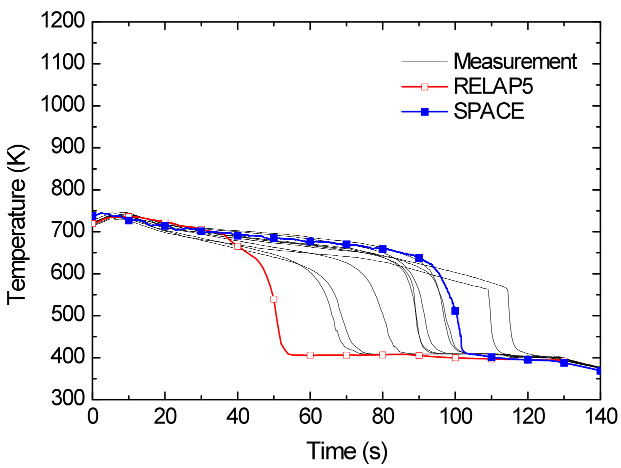

Figure 21. Clad temperature at 10 ft

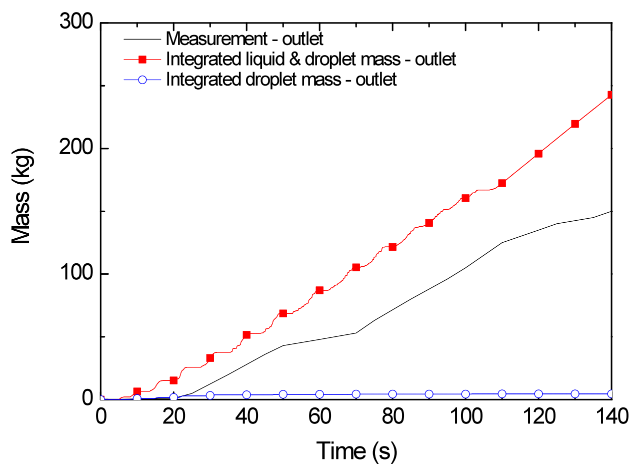

Figure 22. Clad Carryout liquid mass

3. Conclusion

The models and correlations of SPACE code for a post-CHF regime were assessed against the FLECHT-SEASET reflood experiment. SPACE reasonably predicts the wall temperature behaviour and quenching time. For low flooding rates, the quenching times agree well with the experiment. However, early quenching is observed for a high flooding case. In the preliminary assessment, a large effect due to a separated droplet field could not be observed. This might be affected by physical models related to the droplet field such as droplet entrainment/de-entrainment, interfacial drag between droplet and gas, droplet interfacial area, etc. The prediction capability of SPACE code will be further improved as more findings related to droplet field are discovered.

ACKNOWLEDGMENTS

This work was supported by the Nuclear Power Technology Development Program of the Korea Institute of Energy Technology Evaluation and Planning (KETEP) grant funded by the Korea Government Ministry of Knowledge Economy.

4. References

[1] S. J. Ha et al., "Development of the SPACE Code for Nuclear Power Plants," Nuclear Engineering and Technology, 43:1, p. 45, 2011.

[2] D. C. Groeneveld et al., "The 2006 CHF Look-up Table," Nuclear Engineering and Design, 237, p. 1909, 2007.

[3] J. J. Carbajo et al., "A Study on the Rewetting Temperature," Nuclear Engineering and Design, 84, p. 21, 1985.

[4] M. J. Thurgood, et al., COBRA/TRAC – A Thermal-Hydraulics Code for Transient Analysis of Nuclear Reactor Vessels and Primary Coolant Systems, NUREC/CR-3046, PNL-4385, Vol. 1, Revision 4, 1983.

[5] D. C. Groeneveld et al., "A Look-up Table for Fully Developed Film Boiling Heat Transfer," Nuclear Engineering and Design, 225, p. 83, 2003.

[6] L. A. Bromley, "Heat Transfer in Stable Film Boiling," Chemical Engineering Progress, 46, pp. 221-227, 1950.

[7] R. P. Forslund and W. M. Rohsenow, "Dispersed Flow Film Boiling," Transactions of the ASME, Journal of Heat Transfer, 90, 1968, pp. 399-407.

[8] K. H. Sun, J. M. Gonxalez-Santalo and C. L. Tien, "Calculations of Combined Radiation and Convection Heat Transfer in Rod Bundles under Emergency Cooling Conditions," J. Heat Transfer, 414, 1976.

[9] G. T. Analytis, "Developmental Assessment of RELAP5/MOD3.1 with Separate Effect and Integral Test Experiment: Model Changes and Options," Nuclear Engineering and Design, Vol.163, pp.125-148, 1996.

[10] P. Coddington and R. Macian, "A Study of the Performance of Void Fraction Correlations Used in the Context of Drift-Flux Two-Phase Flow Models," Nuclear Engineering and Design, Vol.215, pp.199-216, 2002.

[11] D. Bestion, "The Physical Closure laws in the CATHARE code," Nuclear Engineering and Design, Vol.124, pp.229-245, 1990.

[12] R. Clift, J. R. Grace and M. E. Weber, *Bubbles, Drops, and Particles*, Chapter 7, pp.179, Academic Press, New York, 1978.

[13] J. F. Richardson and W. N. Zaki, "Sedimentation and Fluidisation, Part 1," Trans. Instn. Chem. Engrs., Vol.32, pp.35~53. 1954.

[14] M. Ishii and T. C. Chawla, "Local Drag Laws in Dispersed Two-Phase Flow," NUREG/CR-1230, ANL-79-105, Argonne National Laboratory, 1978.

[15] M. J. Loftus, et al., PWR FLECHT-SEASET Unblocked Bundle, Force and Gravity Reflood Task Data Report, NUREG/CR-1532, 1980.